Identification of Pilot Dynamics in a System with a Choice of Feedback Structures

Norihiro Goto* and Takumi Matsuo†
Kyushu University, Fukuoka, Japan

In controlling the altitude of an aircraft, the pilot has a choice of feedback structures: a lead-equalized altitude feedback single loop or a pitch attitude control inner loop. This paper proposes a method by which it is possible to identify the feedback structure actually employed by the pilot and to describe the pilot dynamics in a system having an inner loop. Identification is made by using the autoregressive scheme and the determination of a proper feedback structure is made by examining the correlation of the innovation processes as well as the identified dynamics. Based on a credibility study, the method is applied here to simulator and flight test data. It is shown that the pilot can employ the feedback structure with a pitch attitude control inner loop. The possibility is suggested, however, that during a run the pilot also employs the altitude feedback single loop in a time-sharing manner. When the feedback structure with a pitch attitude inner loop is assumed, it is observed that the often-used hypothesis of the pilot's high-gain characteristics in the inner loop is to some extent inaccurate.

Introduction

ALTITUDE control is very important in tracking the longitudinal flight path of an aircraft with precision. In view of phugoid damping, however, direct feedback of altitude h to the elevator δ_e is not an effective means of controlling altitude. It is assumed that the pilot makes either a lead equalization in the h feedback single loop (D model, see Fig. 1) or a pitch attitude θ control inner loop (I model, Fig. 2). In Figs. 1 and 2, Y_p, Y_{p_h}, and Y_{p_θ} are pilot transfer functions and r_p, r_h, and r_θ pilot remnants. The closed systems of Figs. 1 and 2 are excited by a vertical gust w_g and a command input h_{c_a}. For the feedback structure of Fig. 2, it is often assumed, especially in a landing approach, that the inner loop closure by the pilot is so tight that the inner closed-loop transfer function θ/θ_c, can be approximated as[1]

$$\frac{\theta}{\theta_c} = \frac{Y_{p_\theta} G_{\theta_{\delta e}}}{1 + Y_{p_\theta} G_{\theta_{\delta e}}} \cong 1 \tag{1}$$

where $G_{\theta_{\delta e}}$ is the θ response to the δ_e transfer function. Equation (1) leads to the simplification of the so-called residualization.[2] However, the hypothesis of the inner loop closure by the pilot and Eq. (1) are yet to be tested by identification.

Thus, the paper is aimed at developing a method by which it is possible to 1) determine which feedback structure the pilot actually employs (D or I model) and 2) identify the pilot dynamics in the system with an inner loop. Applying the method to simulator and flight test data, the paper is also aimed at showing the real control features of the pilot concerning items 1 and 2, thereby testing the adequacy of the approximation of Eq. (1).

Presented as Paper 86-2250 at the AIAA Guidance, Navigation and Control Conference, Williamsburg, VA, Aug. 18-20, 1986; received Sept. 17, 1986; revision received March 13, 1987.

*Associate Professor, Department of Aeronautical Engineering. Member AIAA.

†Student, Department of Aeronautical Engineering; currently, Engineer, Japan Air Lines.

Method of Analysis

Identification is made by use of the autoregressive (AR) scheme,[3-5] in which the system of concern is reduced to the feedback structure of Fig. 3. The reduction of Figs. 1 and 2 to Fig. 3 may be readily conducted as follows:

Case 1 (from Fig. 1 to Fig. 3),

$$\Pi(n) = \delta_e(n) \tag{2a}$$

$$\Gamma(n) = h_\epsilon(n),\ h_\epsilon\text{: altitude deviation} \tag{2b}$$

$$[Y_p(B)] = Y_p(B) \tag{2c}$$

$$[G_\delta(B)] = -G_{h_{\delta e}}(B) \tag{2d}$$

$$H_u(B)U(n) = r_p(n) \tag{2e}$$

$$H_v(B)V(n) = h_c(n) - G_{h_g}(B)w_g(n) \tag{2f}$$

Case 2 (from Fig. 2 to Fig. 3)

$$\Pi(n) = \delta_e(n) \tag{3a}$$

$$\Gamma(n) = [h_\epsilon(n)\ \theta(n)]^T \tag{3b}$$

$$[Y_p(B)] = [Y_{p_h}(B)Y_{p_\theta}(B) - Y_{p_\theta}(B)] \tag{3c}$$

$$[G_\delta(B)] = [-G_{h_{\delta_e}}(B)\ G_{\theta_{\delta_e}}(B)]^T \tag{3d}$$

$$H_u(B)U(n) = Y_{p_\theta}(B)r_h(n) + r_\theta(n) \tag{3e}$$

$$H_v(B)V(n) = \begin{bmatrix} h_c(n) - G_{h_g}(B)w_g(n) \\ G_{\theta_g}(G)w_g(n) \end{bmatrix} \tag{3f}$$

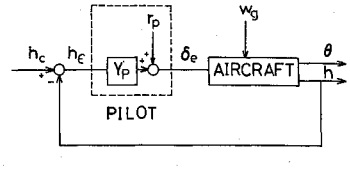

Fig. 1 Direct altitude feedback control loop (D model).

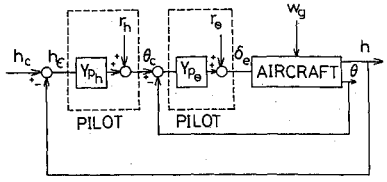

Fig. 2 Altitude control with a pitch attitude control inner loop (I model).

where superscript T denotes the transpose. In Eqs. (2) and (3), n is the sampling instant, $n = 1, 2,\ldots$, and B is the backward shift operator, $B^k y(n) = (n-k)$. $\Pi(n)$ and $\Gamma(n)$ are assumed to consist of zero mean and stationary times series. $G_{h_{\delta_e}}(B)$ is the h response to the δ_e transfer function. $G_{h_g}(B)$ and $G_{\theta_g}(B)$ are h and θ response transfer functions to a vertical gust $w_g(n)$ and $h_c(n)$ is a random fluctuation as the command input. $H_u(B)$ and $H_v(B)$ are shaping filters by which the innovations $U(n)$ and $V(n)$ are turned to actual external noises. $U(n)$ and $V(n)$ should be uncorrelated with each other, as seen from Eqs. (2e), (2f) and (3e), (3f). Equation (3f) also implies that there has to be two mutually uncorrelated external noises in order that the 2×2 matrix $H_v(B)$ is not singular for case 2. From Fig. 3, the closed-loop equation is obtained as

$$\begin{bmatrix}\Pi(n)\\ \Gamma(n)\end{bmatrix} = \begin{bmatrix}0 & [Y_p(B)]\\ [G_\delta(B)] & 0\end{bmatrix}\begin{bmatrix}\Pi(n)\\ \Gamma(n)\end{bmatrix} + \begin{bmatrix}H_u(B) & 0\\ 0 & H_v(B)\end{bmatrix}\begin{bmatrix}U(n)\\ V(n)\end{bmatrix} \tag{4}$$

Solving Eq. (4) for $[\Pi^T\Gamma^T]^T$ yields

$$\begin{bmatrix}\Pi(n)\\ \Gamma(n)\end{bmatrix} = \begin{bmatrix}L_{11}(B) & L_{12}(B)\\ L_{21}(B) & L_{22}(B)\end{bmatrix}\begin{bmatrix}U(n)\\ V(n)\end{bmatrix} \tag{5a}$$

where

$$L_{11}(B) = (I - [Y_p(B)][G_\delta(B)])^{-1}H_u(B) \tag{5b}$$

$$L_{12}(B) = (I - [Y_p(B)][G_\delta(B)])^{-1}[Y_p(B)]H_v(B) \tag{5c}$$

$$L_{21}(B) = (I - [G_\delta(B)][Y_p(B)])^{-1}[G_\delta(B)]H_u(B) \tag{5d}$$

$$L_{22}(B) = (I - [G_\delta(G)][Y_p(B)]^{-1}H_v(B) \tag{5e}$$

In Eq. (5), I is the unit matrix of appropriate dimension. The unknown transfer function matrices $[Y_p(B)]$ and $[G_\delta(B)]$ can be expressed in terms of $L_{ij}(B)$ as

$$[Y_p(B)] = L_{12}(B)L_{22}^{-1}(B) \tag{6a}$$

$$[G_\delta(B)] = L_{21}(B)L_{11}^{-1}(B) \tag{6b}$$

To develop the model of the form of Eq. (5a), a multidimensional AR model is fitted to the observed data vector $X(n) = [\Pi^T(n)\ \Gamma^T(n)]^T$ as[4,6]

$$X(n) = \sum_{m=1}^{M} A(m)X(n-m) + W(n) \tag{7}$$

with

$$E[W(n)] = 0 \text{ (zero vector)} \tag{8a}$$

$$E[W(n)\cdot X^T(n-k)] = 0 \text{ (zero matrix), for } k \geq 1 \tag{8b}$$

$$E[W(n)\cdot W^T(k)] = \delta_{n,k}\Sigma_w,\ \delta_{n,k} = \begin{cases}1, & n=k\\ 0, & n\neq k\end{cases} \tag{8c}$$

where E denotes the expectation, $W(n)$ the estimated innovation vector of $[U^T(n)\ V^T(n)]^T$, and Σ_w the noise covariance matrix of $W(n)$.

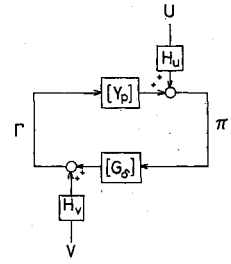

Fig. 3 Closed-loop model suited for the autogreressive scheme.

Letting σ_{ij} be the (i,j) element of Σ_w, the element of the normalized noise covariance matrix is given by $\epsilon_{ij} = \sigma_{ij}/\sqrt{\sigma_{ii}\sigma_{jj}}$. Hereafter, the ith element of $W(n)$ is called the x_i innovation. For instance, the second element of $W(n)$ for both cases 1 and 2 is referred to as the h_ϵ innovation. Therefore, ϵ_{ij} is the normalized correlation between the x_i and x_j innovations. Note that the normalized correlation is thereafter referred to simply as correlation. The unique recoverability of $[Y_p(B)]$ and $[G_\delta(B)]$ by Eq. (6) is guaranteed when $U(n)$ and $V(n)$ are uncorrelated with each other; therefore, Σ_w is a block diagonal, under the condition that the closed-loop system is stable and $[Y_p(0)] = 0$ and $[G_\delta(0)] = 0$.[7] Frequency response functions can be obtained from Eq. (6) by replacing B with $\exp(-j\omega T_s)$, where ω is the frequency in radians/second, T_s the sampling interval in seconds, and $j = \sqrt{-1}$. The AR model of order M in Eq. (7) can be determined by the minimum Akaike's Information Criterion (AIC) procedure.[8]

There are two candidates for feedback structures – the D and I models – one of which is actually employed by the pilot. To distinguish between the two, consider initially what should be obtained for Y_p and r_p of Fig. 1 when the correct structure is the I model. From Fig. 2,

$$\delta_e(n) = Y_{p_\theta}(B)[\theta_c(n) - \theta(n)] + r_\theta(n) \tag{9a}$$

$$\theta(n) = G_{\theta_{\delta_e}}(B)\delta_e(n) + G_{\theta_g}(B)W_g(n) \tag{9b}$$

$$\theta_c(n) = Y_{p_h}(B)h_\epsilon(n) + r_h(n) \tag{9c}$$

Subsituting Eqs. (9b) and (9c) into Eq. (9a) and then solving Eq. (9a) for $\delta_e(n)$ yields

$$\delta_e(n) = Y_p(B)h_\epsilon(n) + r_p(n) \tag{10a}$$

where

$$Y_p(B) = \frac{Y_{p_h}(B)Y_{p_\theta}(B)}{1 + Y_{p_\theta}(B)G_{\theta_{\delta_e}}(B)} \tag{10b}$$

$$r_p(n) = \frac{Y_{p_\theta}(B)r_h(n) - Y_{p_\theta}(B)G_{\theta_g}(B)w_g(n) + r_\theta(n)}{1 + Y_{p_\theta}(B)G_{\theta_{\delta_e}}(B)} \tag{10c}$$

As can be seen in the right-hand side of Eq. (10c), the pilot remnant $r_p(n)$ includes a w_g-related term, which produces a correlation between U and V that should not exist, or practically should be small, if the D model were correct. Therefore, the correlation between the δ_e and h_ϵ innovations for case 1 is expected to become larger than the same correlation for case 2 if the I model is the actual structure employed by the pilot. On the other hand, if the D model is correct, U and V for case 1 must be uncorrelated. In this case, note that there are only two mutually independent noise sources: $r_p(n)$ and $v(n) = [h_c(n) - G_{h_g}(B)w_g(n)]$. Fitting the I model to this case implies that three noise sources are made from only two, $r_p(n)$ and $v(n)$.

Of necessity, this produces the correlation between the δ_e and h_ϵ innovations or a singular H_v when the I model is fitted to the system. Also, Eq. (10b) indicates that employing the I model when the D model is correct corresponds to determining two transfer functions, Y_{p_h} and Y_{p_θ}, from only one Y_p, which cannot be made uniquely and therefore quite likely yields unreasonable Y_{p_h} and Y_{p_θ}. From these considerations, the following four-step procedure is proposed as a means of choosing a proper feedback structure:

1) Perform the D model identification by setting $\Pi(n) = \delta_e(n)$ and $\Gamma(n) = h_\epsilon(n)$.

2) Perform the I model identification by setting $\Pi(n) = \delta_e(n)$ and $\Gamma(n) = [h_\epsilon(n)\ \theta(n)]^T$.

3) Using the results of steps 1 and 2, examine the identified dynamics.

4) Compare the correlation between the δ_e and h_ϵ innovations from step 1 with the same correlation from step 2.

A credibility study[9] using digital simulation data has shown that, as long as the simulation run consists solely of either the D or I model, the method works satisfactorily to check the feedback structure and to identify the unknown plant dynamics in a system with an inner loop.

To be noted here is that a large difference in the correlation of step 4 cannot be expected. When the I model is the correct structure, the reason can be seen if the magnitude of the noise producing the correlation is taken into condsideration. The term in Eq. (10c) that produces the correlation is

$$n_p = \left(\frac{Y_{p_\theta} G_{\theta_g}}{1 + Y_{p_\theta} G_{\theta_{\delta_e}}}\right) w_g = \left(\frac{Y_{p_\theta} G_{\theta_{\delta_e}}}{1 - Y_{p_\theta} G_{\theta_{\delta_e}}}\right) \left(\frac{G_{\theta_g}}{G_{\theta_{\delta_e}}}\right) w_g \qquad (11)$$

while the gust generated noise is from Eq. (2f),

$$n_g = G_{h_g} w_g \qquad (12)$$

By using the transfer functions given in Table 1 for the simulator test (to be discussed in the next section) and by comparing the magnitude of n_p with that of n_g in the frequency range around 1.0 rad/s, it is found that n_p is smaller than n_g by more than 30 dB. When the D model is the correct structure, digital simulation has shown that the correlation difference is almost the same as that shown in the opposite case.

In addition to the individual D and I models, it is possible that the two models are employed alternately in a time-sharing manner during a run (mixed model). A further digital simulation study, which investigated cases having periodic and random alternation, has shown that if the length occupied by one model during a run is larger than about 30% of the total length, the selection indicated by the correlation of step 4 becomes indeterminate and independent of the length ratio. For example, if the total length of the I model is 70% of the run length, the correlation may select the D model. Thus, the selection by step 4 of the proposed procedure may imply the following: a) when the I model is selected, the structure employed by the pilot can be either the I or mixed model, or b) when the D model is selected, it can be either the D or mixed model.

However, it has been shown that the dynamics identified according to the model structure prevailing during a run gives better results, in the sense that the identified dynamics are closer to the simulated ones.

Simulator Test

A series of fixed-base simulator tests was conducted to investigate the human pilot's behavior of controlling altitude. The simulated aricraft was Navion[10]; and the longitudinal small-perturbation equations of motion at a steady flight speed of $V_0 = 176$ ft/s (53.6 m/s) were set on an analog computer. The flight configuration and pertinent transfer functions are given in Table 1, where s is the Laplace transform parameter. A continuous vertical gust w_g having a one-dimensional Dryden spectral form of intensity $\sigma_w = 1.0$ ft/s (0.3 m/s) and scale length $L_w = 460$ ft (140 m) was applied to the aircraft to excite the system. The white noise used to realize w_g had a rms value of 1.0 with a flat power density spectrum up to 500 Hz. A random fluctuation of command h_c was also injected into the system. To realize h_c, a white noise with a rms value of 0.316 and a flat power density spectrum up to 500 Hz was filtered by $1/(1 + 0.5s)$. The time constant of the filter was varied from lower values to 0.5, around which the pilot felt for the first time that he could follow the command without difficulty. The pilot was provided with h_ϵ and θ information through two CRT's. The maximum indication of the h_ϵ display was 8 ft (2.4 m) with the display gain set at 2 ft/div (0.6 m/cm) and that of θ display 11.4 deg with a display gain of 2.86 deg/div. The very high gain of the h_ϵ display selected was considered necessary to cause the pilot to maintain tight control. Longitude was controlled by using the elevator only, which was manipulated by a joy stick having small inertia without a restoring spring. The pilot was told to minimize the altitude deviation h_ϵ.

The subjects were two graduate students, S1 and S2. S1 was a 23 year old with slightly more than 10 h of glider flight experience and S2 a 22 year old with more than 21 h of glider experience. The subjects were trained up until the performance in terms of the mean square altitude error $\overline{h_\epsilon^2}$ for a simulation run lasting about 90 s, which was then decreased to reach an almost constant value. Data runs were conducted after the training. The data length used for the analysis was 61.38 s cut out of about 90 s. The sampling time for converting analog data to digital data was 0.06 s, thereby yielding 1024 data points for each run. Records were taken of elevator deflection angle δ_e (deg), altitude deviation h_ϵ (ft), and pitch attitude angle θ (deg). Results of the analysis will be shown in these units. Results are also shown in the form of open-loop frequency responses. They are for the D model of Fig. 1,

$$h/h_\epsilon(j\omega) = Y_p G_{h_{\delta_e}} \qquad (13)$$

for the inner loop of the I model of Fig. 2,

$$\theta/\theta_\epsilon(j\omega) = Y_{p_\theta} G_{\theta_{\delta_e}} \qquad (14a)$$

and for the outer loop of the I model of Fig. 2,

$$\frac{h}{h_\epsilon}(j\omega) = Y_{p_h}\left(\frac{G_{h_{\delta_e}}}{G_{\theta_{\delta_e}}}\right)\left(\frac{G_{\theta_{\delta_e}} Y_{p_\theta}}{1 + G_{\theta_{\delta_e}} Y_{p_\theta}}\right) \qquad (14b)$$

The pilot and aircraft frequency responses in Eqs. (13) and (14) are identified by use of Eq. (6). In figures showing the open-loop frequency responses during the simulator test, points indicate the means across runs and vertical lines the ranges of variation at a particular frequency.

Simulator Test Results

A set of results for subject S1 is shown first. Going through the aforementioned steps 1–4 may suggest which model is appropriate to each run – D or I. The simulator test for S1 consisted of six data runs. However, analysis revealed that, for three out of six runs, the correlation between U and V was so large that identification in the form of Fig. 3 was not successful. Results for the remaining three runs are shown in order of steps 1–4.

In Fig. 4 are exhibited the identified results of Y_p when the D model is assumed. The next step yields Fig. 5 where the identified results for the I model are shown. The pilot dynamics given in Fig. 4 generally show lead characteristics in a low-frequency range, but with a considerable phase lag. The result for run 2 in Fig. 4 is most unusual, while the corresponding result of run 2 according to the I model (as seen in Fig. 5) shows quite smooth and almost pure gain pitch control characteristics for the inner loop and a first-order lag with a slight lead in the high-frequency range for the outer

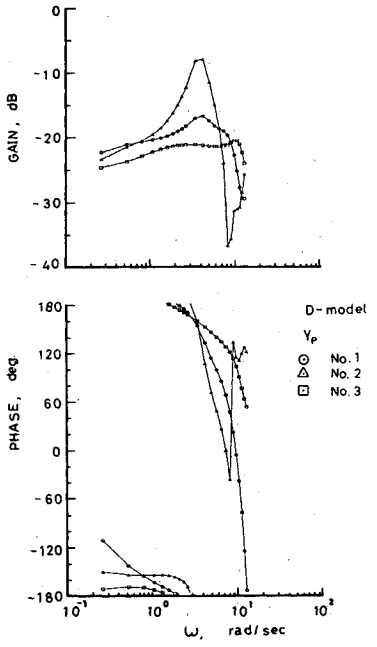

Fig. 4 Identified pilot describing functions for the subject S1: Y_p of D model.

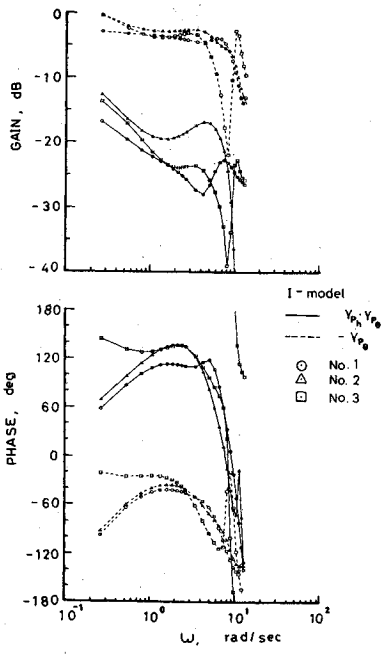

Fig. 5 Identified pilot describing functions for the subject S1: $Y_{p_h} \cdot Y_{p_\theta}$, $-Y_{p_\theta}$ of D model.

loop. Stability analysis of the I model, assuming a pure gain Y_{p_h} and a first-order lead Y_{p_θ}, can show that the magnitude of Y_{p_h} gain must be small (around -10 dB) to attain satisfactory closed-loop damping, so that the relative magnitude of Y_{p_θ} should be much higher than that of $Y_{p_h} \cdot Y_{p_\theta}$. Taking these into account, the describing function shown in Fig. 5 seems more likely to be employed by the pilot than that shown in Fig. 4, as far as run 2 is concerned. Similar features are observed also for runs 1 and 3, although not as distinctly as for run 2.

Checking step 4 substantiates that, for these three runs, the I model may be more appropriate than the D model, although there is the possibility that the mixed model is employed. Table 2 gives the normalized noise covariance matrix for run 2. It is seen that the correlation between the δ_e and h_ϵ innovations for the D model (0.248) is larger than that for the I model (0.227). Similar correlation characteristics are obtained for runs 1 and 3. Figures 6 and 7 show the open-loop frequency responses: Fig. 6 for h/h_ϵ of the D model and Fig. 7 for θ/θ_ϵ and h/h_ϵ of I model. Both show the average over three runs. It is seen that h/h_ϵ of the D model shown in Fig. 6 is very similar to the corresponding one in Fig. 7. Table 3 tabulates the inner- and outer-loop features, performance in terms of rms value of h_ϵ, and the order M of the fitted AR model of Eq. (7) for the I model analysis. The results for subject S2 and the pilot for the flight test are also shown in Table 3. Clearly, from these figures and table, the closed system is stable enough. However, as seen from Fig. 8, which shows the inner closed-loop frequency response θ/θ_c for both subjects S1 and S2, the bandwidth (BW) of the inner loop is very limited: about 1.7 rad/s if the definition of BW is the frequency at which the phase angle of θ/θ_c is -90 deg and even lower if BW is defined to be the frequency where $|\theta/\theta_c| = -3$ dB.

The average performance of the three runs for S1, as obtained from Table 3, is 0.750 ft. This value is much better than the average value of 1.47 ft of the three runs for which the identification was not successful. These performance characteristics may suggest that the control method S1 employed for these three runs had some advantage over the one he used for the rest. Note that the performance for run 2 is the best of all six runs for S1.

Twelve data runs were conducted with subject S2. With regard to the correlation between U and V, identification was judged successful for all the 12 runs. Taking steps 1-3 suggested that, for 9 of the 12 runs, describing functions defined by the I model were more reasonable to this subject than those of the D model. Checking step 4 revealed, however, that the number of runs for which the D model was regarded as appropriate was the same as that for which the I model was appropriate. Only the I model results according to step 4 are shown here: Fig. 8 for the inner closed-loop frequency response functions and Fig. 9 for the open-loop describing functions. Note that the results of Figs. 8 and 9 for S2 are averaged over five runs. Run 6 shows a tendency very different from the other five and is not included in the average.

Table 1 Flight configuration and pertinent transfer functions for simulator test[a]

V_0 = steady-state velocity, = 176 ft/s (53.6 m/s)
α_0 = angle of attack at trim, = 0.6 deg
γ_0 = flight-path angle, = 0 deg

$$\theta/\delta_e = -11.0(s + 0.0523)(s + 1.92)/\Delta$$
$$h/\delta_e = 28.2(s + 0.0165)(s + 13.1)(s - 10.1)/s\Delta$$
$$\theta/w_g = (-0.00664s^3 + 0.0257s^2 + 0.00102s)/\Delta$$
$$h/w_g = -(2.02s^3 + 8.51s^2 + 0.356s + 0.595)/s\Delta$$
$$\Delta = (s^2 + 2 \times 0.696 \times 3.61s + 3.61^2)(s^2 + 2 \times 0.0801 \times 0.214s + 0.214^2)$$

[a]Notes: δ_e and θ in radians; h in feet.

Table 2 Normalized noise covariance matrix of run 2 with subject S1

D model

	δ_e	h_ϵ
δ_e	1.0	0.248
h_ϵ	0.248	1.0

I model

	δ_e	h_ϵ	θ
δ_e	1.0	0.227	−0.319
h_ϵ	0.227	1.0	−0.322
θ	−0.319	−0.322	1.0

Table 3 Inner- and outer-loop characteristics of *T* model for simulator and flight tests[a]

Subject	Run	AR model order	Inner loop ω_c, rad/s	Inner loop φ_M, deg	Inner loop g_M, dB	Outer loop g_M, dB	Performance, ft
	1	19	0.97	66.5	10.0	10.0	0.721
S1	2	18	0.0	80.0	8.5	9.0	0.718(1.11)
	3	17	0.5	106.0	16.7	NA	0.812
	1	17	0.42	144.0	15.5	8.0	2.76
	2	8	0.61	60	14.0	5.2	1.45
S2	3	19	NA	NA	16.0	5.5	0.818(1.56)
	4	8	NA	NA	25.4	4.8	1.06
	5	8	NA	NA	33.0	8.0	1.22
	6	13	0.31	68.0	28.5	43.0	1.30
Research	1	5	0.42	86.0	18.5	18.0	7.80
pilot	2	5	NA	NA	12.0	11.7	18.4

[a] Notes: ω = crossover frequency; φ = phase margin; g_M = gain margin; NA = not available

Performance $= \left[\frac{1}{N}\sum_{i=1}^{N}(h_\epsilon(i) - \bar{h}_\epsilon)^2\right]^{1/2}$

$\bar{h}_\epsilon = \frac{1}{N}\sum_{i=1}^{N} h_\epsilon(i)$

( ) = average over total runs, 6 for S1 and 12 for S2

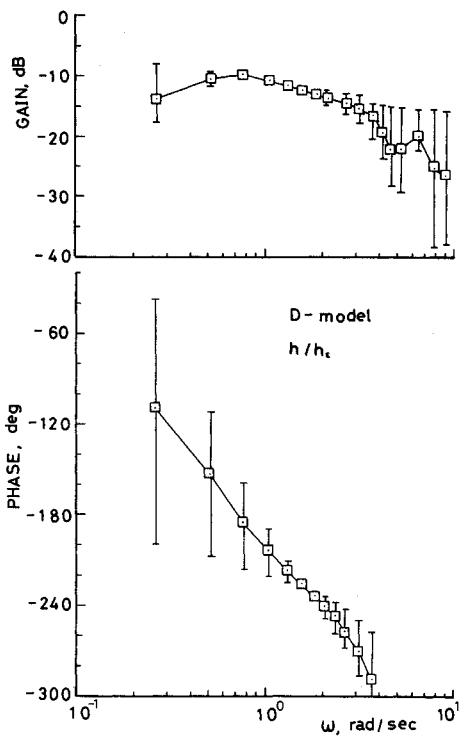

Fig. 6 Open-loop describing functions for the subject S1: h/h_ϵ of D model.

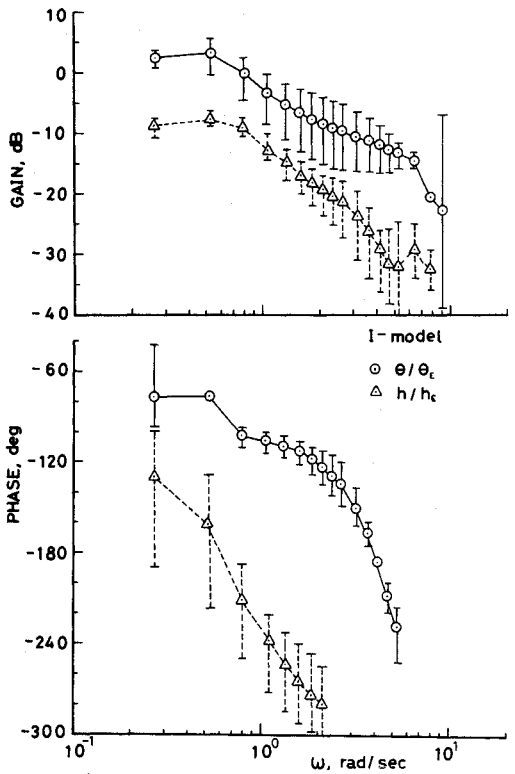

Fig. 7 Open-loop describing functions for the subject S1: θ/θ_ϵ and h/h_ϵ of I model.

It is found that subject S2 takes a lower gain level of the inner loop than S1. This is reflected in Fig. 8, which shows that the frequency range where the θ/θ_c gain is near 0 dB is so limited that S2 finds it more difficult to accept the approximation of Eq. (1) than S1. One explanation for this is that use of step 4 split the analyzed data equally into the D and I model groups; thus, subject S2 employed the mixed model throughout this series of experiments. From the performance point of view, it is interesting to find that the correlation generally picks up the runs for which the performance is better than the average. For the six runs shown in Table 3, the average performance is 1.43 ft, while the average over the six runs for which the correlation indicates the D model is 1.69 ft, as compared with the average over all 12 runs of 1.56 ft. The relationship between performance and loop structure selected by the correlation must be studied further.

Flight Test

The data were obtained in a series of flight tests for the evaluation of a flight control system to implement a variable stability and response airplane (VSRA) concept.[11] The data used here are, however, for the evaluation of flights with the flight control system disengaged. The aircraft has a twin-piston engine, a gross weight of about 33.3 kN, and a fly-by-wire control system, thus, the aircraft indicated in Figs. 1 and 2 include the dynamics of control surface servoactuators. The

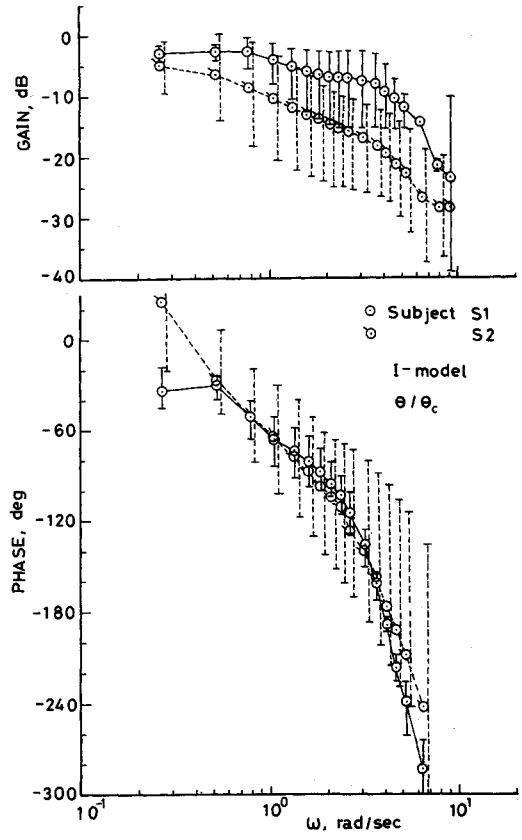

Fig. 8 Inner closed-loop frequency response functions: θ/θ_c of I model for subjects S1 and S2.

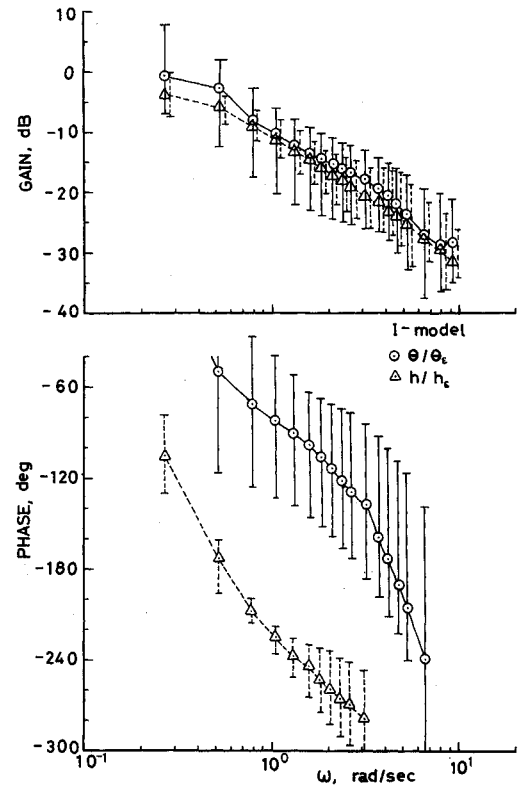

Fig. 9 Open-loop describing functions for the subject S2: θ/θ_ϵ and h/h_ϵ of I model.

flight configuration was glideslope tracking by visual flight rules (VFR) in the landing approach phase from a 2500 ft (760 m) altitude along a 1.5 deg glide slope while maintaining IAS at 120 mph (53.6 m/s). Table 4 summarizes the longitudinal flight conditions, pitch and altitude response transfer functions to elevator and vertical gust with respect to a body-axis system, and elevator servoactuator dynamics. The pilot's real output (wheel stroke in a length dimension) is linearly related to elevator position δ_{em} in the static sense. The converted pilot output δ_{em} is then related dynamically to the real elevator position δ_e by the servoactuator dynamics. Note that the describing functions to appear later are the relations between δ_{em} and the error information, h_ϵ or θ_ϵ. All of the information provided to the pilot was digitally processed to eliminate noise, and was displayed on conventional instruments. As a result of the digital processing, however, the random fluctuation of command h_c shown in Figs. 1 and 2 was ignored. Instead, a turbulence component u_g along the X axis existed in addition to w_g. These two turbulence components are considered to be orthogonal to each other, so that there are enough independent noise sources even for the I model identification. It is not difficult to derive the relationships corresponding to Eqs. (2f) and (3f) for the case without h_c but with u_g. It should be noted that the gain of the glide slope deviation indicator at the outer-marker point was 40 m/dot, which is very low when compared with the gain employed in the simulator tests. The pilot was experienced in research flight, had an instrument rating, and had flown over 1500 h in aircraft used for this test.

Results of flight test runs 1 and 2 are shown here. The data length for the analysis was carefully selected so that it consisted only of the portion in which no throttle movement was employed by the pilot. Thus, the data length is dependent on the run; 60 s for run 1 and 80 s for run 2. The sampling interval was 0.125 s.

Table 4 Flight configuration and pertinent transfer functions for flight test[a]

V_0 = steady-state velocity = 58.7 m/s (192.6 ft/s)
α_0 = angle of attack at trim = 7.4 deg
γ_0 = flight-path angle = -1.5 deg

$$\theta/\delta_e = -11.7(s+0.880)(s+0.0862)/\Delta$$
$$h/\delta_e = 15.8(s+0.0308)(s+6.74)(s-5.79)/s\Delta$$
$$\theta/w_g = -(0.0511s^3+0.0510s^2+0.00397s)/\Delta$$
$$h/w_g = -(0.945s^4+4.01s^3+10.0s^2+0.104s+0.208)/s\Delta$$
$$\Delta = (s^2+2\times0.752\times2.65s+2.65^2)\times(s^2+2\times0.156\times0.173s+0.173^2)$$

Elevator servoactuator dynamics

$$\delta_e/\delta_{em} = 6.28^2/(s^2+2\times0.7\times6.28s+6.28^2)$$

[a]Notes: δ_{em} is the pilot output converted to equivalent elevator deflection angle in radians; δ_e and θ in radians; h in meters.

Flight Test Results

The results are shown in the form of open-loop describing functions and the inner closed-loop frequency response functions. It is found from Table 5, which shows the normalized noise covariance matrix for run 1, that the situation of the correlation between U and V is not very good. Various factors could contribute to this situation; e.g., velocity control made by the elevator, nonstationary pilot control behavior, nonstationary turbulence characteristics along the flight path, information acquisition by VFR, etc. For run 2, the correlation between U and V is even worse than for run 1, indicating that the D model was used. With these factors in mind, the I model was fitted to these two runs to yield Fig. 10, which shows the open-loop describing functions, and Fig. 11 showing the inner closed-loop frequency response functions. Note that the $[Y_p]$ and $[G_\delta]$ of Eqs. (3c) and (3d)

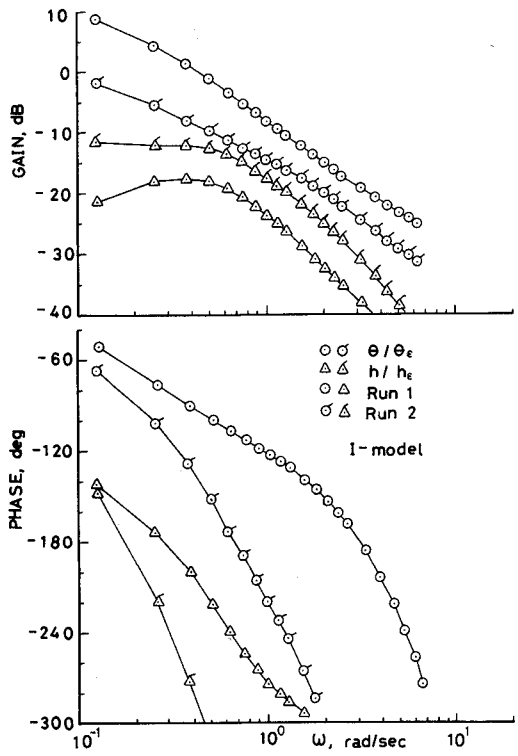

Fig. 10 Open-loop describing functions for flight test runs 1 and 2: θ/θ_ϵ and h/h_ϵ of I model.

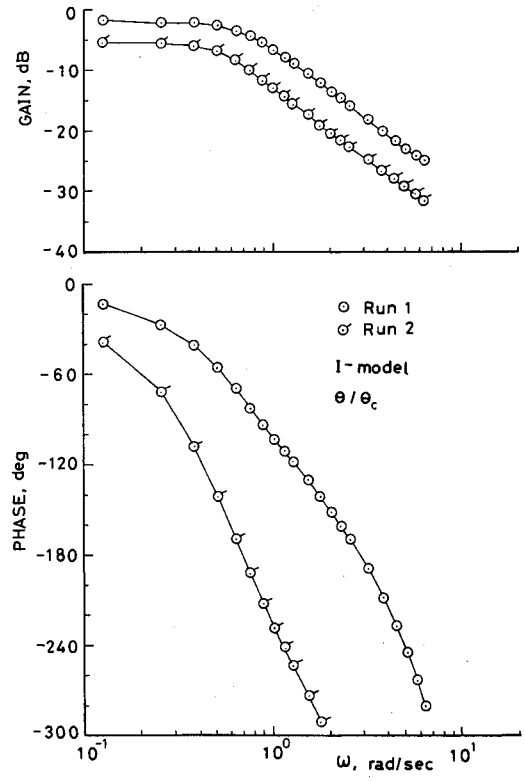

Fig. 11 Inner closed-loop frequency response functions: θ/θ_c of I model for the flight test runs 1 and 2.

Table 5 Normalized noise covariance matrix for flight test, run 1

	D model	
	δ_e	h_ϵ
δ_e	1.0	−0.317
h_ϵ	−0.317	1.0

	I model		
	δ_e	h_ϵ	θ
δ_e	1.0	−0.302	−0.437
h_ϵ	−0.302	1.0	0.770
θ	−0.437	0.770	1.0

used to compute these results are those identified by use of Eq. (6), as in the simulator test case.

The inner-loop frequency response θ/θ_ϵ for run 1 as shown in Fig. 10 exhibits typical characteristics of the crossover model,[12] although the crossover frequency as given in Table 3 is lower and the estimated time delay of about 0.5 s is larger than those generally used for single-loop analyses. For run 2, there are indications that the external noise characteristics were different from those for run 1: the variation in forward speed is larger for run 2 than for run 1 and the elevator movements show different characteristics.

It should be mentioned that the existence of servoactuator dynamics causes a stability problem in the inner loop of Fig. 2. Assuming pilot dynamics of the form $Y_{p_\theta} = K(1 + Ts)$, where T is the lead time constant, a stability analysis can show that for small T the open-loop gain at the stability limit is about 56 dB, while for an appropriately large T, say $T = 0.2$ s, it is about 64 dB. It is readily seen that the pilot control for both runs 1 and 2 is well within these limits. The pilot can take higher gains in the inner loop to make the bandwidth wider than that shown in Fig. 11. The factors that prevented the pilot from taking a higher gain should be investigated further.

In general, the outer-loop characteristics are seen to be similar to those found by subject S1 during the simulator test. Low-frequency control and low-gain characteristics in the outer loop are well shown. However, these low-frequency and low-gain features in the outer loop make the analyses of real flight data rather difficult. More careful design of the experimental situation seems to be necessary.

Conclusion

A statistical method using the autoregressive scheme has been applied to determine pilot control behavior in an altitude control system in which the pilot has a choice of feedback structures. The analyses of simulator and flight test data have indicated that the pilot may employ the feedback structure with a pitch attitude control inner loop and that there is a possibility that during a run the pilot also employs the altitude feedback single loop in a time-sharing manner. When the feedback structure with a pitch attitude control inner loop is assumed, the tightness of the pilot's pitch attitude control in the inner loop is limited in the frequency range and in that the inner closed-loop frequency response function is accompained by a large phase lag. The often-made approximation that the inner pitch control closed-loop transfer function is equal to unity should be used carefully when control is made manually.

It must be noted that there may be other factors contributing to the run-to-run variability shown in this work, but that the test methodology cannot detect. For example, the subjects used in the simulator test probably did not have sufficient flight experience to select the correct control strategy to use. Evaluation these factors to improve the methodology of the testing is being undertaken.

Acknowledgment

This research was supported by a Grant-in-Aid for Developmental Scientific Research of the Ministry of Education of Japan and the International Fund of the Faculty of Engineering, Kyushu University. The authors acknowledge M. Komoda, N. Kawahata, Y. Tsukano, and T. Ono of the Flight Research Division, National Aerospace Laboratory, Japan, for use of their data, as well as valuable discussions.

References

[1]Franklin, J.A., Innis, R.C., Hardy, G.H., and Stephenson, J.D., "Design Criteria for Flightpath and Airspeed Control for the Approach and Landing of STOL Aircraft," NASA TP-1911, 1982.

[2]Stengel, R.F. "A Unifying Framework for Longitudinal Flying Qualities Criteria," *Journal of Guidance, Control, and Dynamics,* Vol. 6, March-April 1983, pp. 84-90.

[3]Shinners, S.M., "Modeling of Human Operator Performance Utilizing Time Series Analysis," *IEEE Transactions of Systems, Man, and Cybernetics,* Vol. SMC-4, Sept. 1974, pp. 446-458.

[4]Goto, N., "A Statistical Method Applied to Pilot Behavior Analysis in Multiloop Systems," *Journal of Guidance and Control,* Vol. 3, Jan-Feb. 1980, pp. 62-68.

[5]Biezad, D.J. and Schmidt, D.K., "Normalized Predictive Deconvolution: A Time Series Algorithm for Modeling Human Operator Dynamics," *Journal of Guidance, Control, and Dynamics,* Vol. 8, Nov.-Dec. 1985, pp. 768-776.

[6]Akaike, H., Arahata, E., and Ozaki, T., "TIMSAC-74: A Time Series Analysis and Control Program Package," Pts. 1 and 2, *Computer Science Monographs,* Institute of Statistical Mathematics, Tokyo, March 1975 and Feb. 1976.

[7]Ng, T.S., Goodwin, G.C., and Anderson, B.D.O., "Identifiability of MIMO Linear Dynamic Systems Operating in Closed Loop," *Automatica,* Vol. 13, 1977, pp. 477-485.

[8]Akaike, H., "A New Loop at the Statistical Model Identification" *IEEE Transactions on Automatic Control,* Vol. AC-19, Dec. 1974, pp. 716-723.

[9]Goto, N., "On a Method for Pilot Dynamics Identification Reflecting Feedback Structures," *Technology Reports of the Kyushu University,* Vol. 58, No. 6, 1985, pp. 985-991 (in Japanese).

[10]Teper, G.L., "Aircraft Stability and Control Data," Systems Technology Inc., Hawthorne, CA, TR 176-1, 1969.

[11]Komoda, M., Kawahata, N., Tsukano, Y., and Ono, T., "Variable Stability and Response Airplane (VSRA) System and Its Flight Verification (I) and (II)," *Journal of the Japan Society for Aeronautical and Space Sciences,* Vol. 31, No. 349, 1983 (in Japanese).

[12]McRuer, D.T. and Jex, H.R., "A Review of Quasi-Linear Pilot Models," *IEEE Transactions on Human Factors in Electronics,* Vol. HFE-8, No. 3, Sept, 1967, pp. 231-249.